Frontiers of Physics
https://doi.org/10.1007/s11467-020-1019-8
Front. Phys.
16(3), 32501 (2021)

RESEARCH ARTICLE

Laser cooling with adiabatic passage for type-II transitions

Qian Liang[1], Tao Chen[1,†], Wen-Hao Bu[1], Yu-He Zhang[1], Bo Yan[1,2,3,‡]

[1] *Interdisciplinary Center of Quantum Information, State Key Laboratory of Modern Optical Instrumentation, Zhejiang Province Key Laboratory of Quantum Technology and Device, Department of Physics, Zhejiang University, Hangzhou 310027, China*
[2] *Collaborative Innovation Centre of Advanced Microstructures, Nanjing University, Nanjing 210093, China*
[3] *Key Laboratory of Quantum Optics, Chinese Academy of Sciences, Shanghai 200800, China*
Corresponding authors. E-mail: †phytch@zju.edu.cn, ‡yanbohang@zju.edu.cn
Received August 3, 2020; accepted October 15, 2020

We extend the idea of laser cooling with adiabatic passage to multi-level type-II transitions. We find the cooling force can be significantly enhanced when a proper magnetic field is applied. That is because the magnetic field decomposes the multi-level system into several two-level sub-systems, hence the stimulated absorption and stimulated emission can occur in order, allowing for the multiple photon momentum transfer. We show that this scheme also works on the laser-coolable molecules with a better cooling effect compared to the conventional Doppler cooling. A reduced dependence on spontaneous emission based on our scheme is observed as well. Our results suggest this scheme is very feasible for laser cooling of polar molecules.

Keywords laser cooling of polar molecule, adiabatic passage, type-II transition, cold molecule, cold atom

1 Introduction

Allowing fast producing and precise manipulation of cold atomic samples [1–3], laser cooling technique has revolutionized the field of atomic, molecular, optical and quantum physics during last several decades [4–8]. For conventional Doppler cooling on atoms such as alkali atoms, the main cooling laser is typically red-detuned with only single frequency (without consideration on the repump laser). It is good enough for most laser-coolable atomic species. But for some special cases, multi-frequency cooling schemes [9], including adiabatic rapid passage [10–12] and bichromatic force [13–16], have been proposed and predicted to have a better performance, but with the price of increasing the complexity of the system. However, some features, for example, stronger cooling forces and a weak dependence on spontaneous emission [9], make them potentially be applied to direct laser cooling of molecules where the cooling transition is quasi-closed [17–20]. Besides the leakage channels, the energy levels for molecules are complicated and the type-II transitions (in which the total angular momentum quantum number in the ground state J is no less than that in the excited state J') are dominant [21, 22], making the cooling process much more complex and the Doppler cooling force much weaker than those in atoms. To achieve a better cooling efficiency, it might be worthwhile to sacrifice the simplicity of the cooling scheme by introducing a light field with multiple frequencies [23].

The mechanism of laser cooling can be explained with an atom-light interaction approach in either semi-classical or quantum picture [24–26]. Briefly speaking, in Doppler cooling process, the momentum from photons is transferred to atoms by scattering the photons. The Doppler effect breaks the symmetry in the momentum space, making the atoms focus to the zero momentum [24]. The strength of the cooling force depends on how fast the momentum exchange is repeated, that is, the decay rate from the excited state. Once successive scattering is achieved in a closed cycling transition, the force would only be limited by the spontaneous decay rate Γ. For a two-level system, the maximum force is $F_{\max} = \hbar k\Gamma/2$ with $\hbar k$ the photon momentum. The cooling velocity range and the temperature limit also depend on the decay rate Γ [24].

One way to go beyond the limit of the spontaneous emission is using the stimulated emission[27]. Recently, an adiabatic-passage cooling scheme by rapidly sweeping the laser frequency in a sawtooth wave shape (Sawtooth-wave adiabatic passage, or SWAP, for short) has been theoretically and experimentally demonstrated in narrow-line transitions [28–31]and Raman transitions [32]. Such a scheme uses the stimulated emission to transfer the excited atoms back to the ground state, therefore strong

*arXiv: 1902.05212. This article can also be found at http://journal.hep.com.cn/fop/EN/10.1007/s11467-020-1019-8.

forces can be achieved with a high sweeping rate even for a narrow transition. Let us consider a moving particle with a velocity of v in a light field, which is formed by two counter-propagating laser beams with the same time-dependent frequency $\omega(t)$; see Fig. 1(a). Due to the Doppler effect, resonances of the particle with the two beams happen at different time. For a frequency ramping scheme shown in Fig. 1(b), an adiabatic excitation is first induced by the counter-propagating beam, followed by another adiabatic de-excitation process induced by the co-propagating beam. Ideally, the particle loses twice the photon momentum during one sweeping period, resulting in a maximum average force of $F_{\mathrm{SWAP}} = 2\hbar k T^{-1}$ with T the sweep time in one period. To guarantee the adiabatic transfer, the Landau–Zener condition $\Omega^2 \gg \alpha$ should be fulfilled [33], here Ω is the Rabi frequency and $\alpha \equiv \frac{\mathrm{d}\omega}{\mathrm{d}t}$ is the frequency ramp speed.

Now an interesting question is whether the SWAP scheme can be extended to multi-level type-II transitions and further complex molecules. The type-II transitions generally show a weak Doppler cooling force [34, 35] due to the remixing process of the dark states via either rapidly switching the polarization of the light [18, 36] or introducing a magnetic field that has an angle to the laser beams to re-define the quantum axis [17, 37]. Here we consider the latter case. Different from the ideal two-level system, the problem of the multi-level systems lies in that the excitation and stimulated de-excitation pairs might happen out of order. The three polarization components of the two beams take part in the interaction, and therefore lead to the lost of the resonance order. This will degrade the efficiency of the momentum transfer.

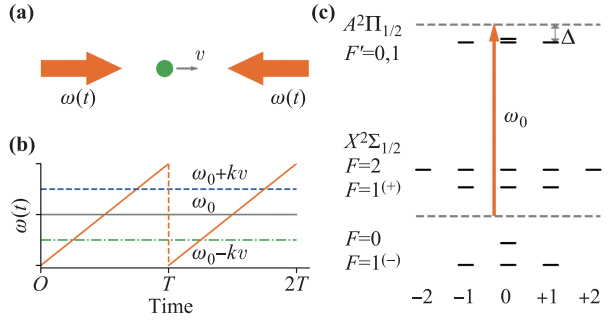

Fig. 1 **(a)** Laser cooling scheme with sawtooth wave adiabatic passage. The two counter-propagating laser beams with a time-dependent frequency of $\omega(t)$ interact with a moving particle with a velocity of v. **(b)** The laser frequency $\omega(t)$ ramps linearly in one sweeping period T. Due to the Doppler effect, the two beams become resonant with the moving particle at different times associated with the green dotted dashed line (counter-propagating) and the blue dashed line (co-propagating). The gray solid line represents the center frequency ω_0 of the sweeping. **(c)** The typical 4+12 hyperfine structure for laser coolable diatomic molecules. The energy gap between the two dashed lines indicates the center frequency ω_0 of the chirped laser beams in (b). Note that the bottom dash line is the center energy position of the four ground hyperfine states. Δ is the corresponding detuning between ω_0 and the transition frequency.

Lots of molecules that have been directly laser cooled, such as ^{88}SrF, ^{40}CaF, have a 4+12 hyperfine structure (under weak magnetic field), i.e., there are 4 sublevels in the $A^2\Pi_{1/2}$ state and 12 sublevels in the $X^2\Sigma_{1/2}$ state, as illustrated in Fig. 1(c). It makes the momentum transfer much more complicated. In this work, we apply a time-dependent master equation approach to deal with the interaction between a multi-level system and a frequency-chirped light field for the one-dimensional case. Then, we investigate the SWAP cooling effect for type-II transitions in Section 3, where the motion of the particles is classically treated. Note that our work is different from the discussion on the Raman transition in Ref. [32] where the frequency ramp is much narrower than the ground-state splitting, and so they require an explicit optical pumping step to reinitialize the state matrix before every frequency ramp. Here we use the frequency ramp that covers the entire hyperfine manifold and addresses all sublevels in each ramp. Next we implement the SWAP scheme on the molecule to analyze its cooling effect in Section 4. Finally, in Section 5, we consider a three-level model with one dark state to check the resistance of the SWAP scheme on the unwanted loss channels.

2 Time-dependent master equation approach

2.1 Semi-classical treatment

Without loss of generality, we consider the interaction between a multi-level particle and a multi-frequency laser field. An arbitrary multi-frequency light field can be decomposed as

$$\boldsymbol{E} = \sum_{n,q} \frac{1}{2} E_n M_{nq} \hat{\epsilon}_q \mathrm{e}^{\mathrm{i}\boldsymbol{k}_n \cdot \boldsymbol{z}} \mathrm{e}^{-\mathrm{i}\beta_n(t)} + c.c., \tag{1}$$

where n is the laser beam index with frequency ω_n and wave vector (propagating direction) $\boldsymbol{k}_n$, and E_n is the amplitude of the n-th beam. The wave number k_n here can be approximately treated as constant for simplicity. $q = 0, \pm 1$ correspond to π, $\sigma^{\pm}$ polarizations respectively. The polarization vectors under the Cartesian coordinate axis are: $\hat{\epsilon}_0 = \hat{e}_z$, $\hat{\epsilon}_{\pm} = \mp(\hat{e}_x \pm \mathrm{i}\hat{e}_y)/\sqrt{2}$. Here the Cartesian coordinate is assumed to have a specific orientation to the laser beam. $|M_{nq}|^2$ gives the intensity fraction of the light field for each polarization component in the n-th beam. $\beta_n(t) \equiv \int_{t_0}^{t} \omega_n(t')\mathrm{d}t'$ is the accumulated phase of the n-th laser beam from the initial time t_0.

Using Eq. (1), the Hamiltonian in the interaction picture is

$$H = \frac{\hbar}{2} \sum_{u,l} \sum_{n,q} \Omega_{ul}^{nq} |u\rangle\langle l| + h.c., \tag{2}$$

with $|l\rangle$ and $|u\rangle$ represent the ground and excited states respectively, and

$$\Omega_{ul}^{nq} = \mathrm{e}^{\mathrm{i}\boldsymbol{k}_n\cdot\boldsymbol{z}}\mathrm{e}^{-\mathrm{i}\Theta_{nq}^{ul}(t)}M_{nq}A_{ul}^{(q)}\Omega_n. \tag{3}$$

Here Ω_n is the total Rabi frequency of the n-th beam. $\Theta_{nq}^{ul}(t) \equiv \int_{t_0}^{t}[\omega_n(t')-\omega_{ul}+\delta_{ul}(B)]\mathrm{d}t'$ is the time-dependent phase of the laser detuning. $\omega_n(t)$ has a sawtooth shape versus t as shown in Fig. 1(b), and ω_{ul} is the resonant frequency for the $|l\rangle \to |u\rangle$ transition. $\delta_{ul}(B) = \delta_l(B) - \delta_u(B)$, where $\delta_{l(u)}(B)$ is the energy shift of the sublevel $|l\rangle(|u\rangle)$ under a magnetic field with strength of B. $A_{ul}^{(q)}$ are the relative transition strengths for all electric dipole allowed transitions.

The force can be derived from the gradient of the total energy of the system, that is,

$$\hat{F} = -\nabla H = -\frac{\hbar}{2}\sum_{u,l}\sum_{n,q}(\nabla\Omega_{ul}^{nq})|u\rangle\langle l| + h.c., \tag{4}$$

then the expectation value of the force for a system represented by a density matrix ρ is $\langle F\rangle = \mathrm{Tr}(\rho\hat{F})$. The motion of the particles is treated classically. By letting $z = vt$ in Eq. (3), the Hamiltonian (2) and thus the force operator (4) become velocity dependent.

The time evolution of the density matrix ρ is determined by the master equation

$$\frac{\partial\rho}{\partial t} = \frac{1}{\mathrm{i}\hbar}[H,\rho] + \hat{\mathcal{L}}(\rho), \tag{5}$$

where the Linblad operator

$$\hat{\mathcal{L}}(\rho) = \frac{1}{2}\sum_{ul}(2C_{ul}\rho C_{ul}^{\dagger} - C_{ul}^{\dagger}C_{ul}\rho - \rho C_{ul}^{\dagger}C_{ul}) \tag{6}$$

with the collapse operator $C_{ul} = \sum_q A_{ul}^q\sqrt{\Gamma}|l\rangle\langle u|$. We start with an initial state and evolve the system in time until the density matrix finally changes periodically with the frequency sweeping. Then we calculate the average force over one SWAP ramp period T.

2.2 Remixing of the Zeeman dark state

For laser cooling with the type-II transitions and molecules, a magnetic field B is introduced to eliminate the dark states. The direction of the magnetic field redefines the local quantum axis. We assume the field is on the lab coordinate yz plane and has an angle of θ to the z axis. So the Cartesian components of the polarization vector $\hat{\epsilon}_{0,\pm}$ is rotated by transforming from $\{\hat{e}_x,\hat{e}_y,\hat{e}_z\}$ of the old frame to $\{\hat{e'}_x,\hat{e'}_y,\hat{e'}_z\}$ of the re-defined frame. The new M vector for the three polarizations in each laser beam can be obtained from the old one, i.e.,

$$\begin{pmatrix}M'_{+1}\\M'_0\\M'_{-1}\end{pmatrix} = \frac{1}{2}\begin{pmatrix}1+\cos\theta & \sqrt{2}\sin\theta & 1-\cos\theta\\ -\sqrt{2}\sin\theta & 2\cos\theta & \sqrt{2}\sin\theta\\ 1-\cos\theta & -\sqrt{2}\sin\theta & 1+\cos\theta\end{pmatrix}\begin{pmatrix}M_{+1}\\M_0\\M_{-1}\end{pmatrix}. \tag{7}$$

In our calculations below, we consider the one-dimensional case that the particle moves along $\hat{z}$-axis for simplicity. A light field from two counter-propagating beams in σ^+–σ^- configuration [the polarization here is defined by the lab $\hat{z}$-axis before the transformation with Eq. (7)] is applied, and the two beams have an equal Rabi frequency Ω. When the magnetic field is carefully chosen ($\theta \neq 0$), they contain all three polarization components and thus can effectively eliminate all of the Zeeman dark states. We first investigate the possible type-II transitions in Fig. 1(c) under a weak magnetic field, and then turn our attention to strong magnetic field regime.

3 SWAP cooling for type-II transitions

A typical 4+12 energy structure for the diatomic molecule is shown in Fig. 1(c), there are three different multi-level type-II transitions: (i) $F = 1 \to F' = 0$, (ii) $F = 1 \to F' = 1$ and (iii) $F = 2 \to F' = 1$. We first focus on the case (i) and use the parameters for the $F = 1^{(-)} \to F' = 0$ transitions for the typical laser coolable diatomic molecule (in our case, it is BaF, but the conclusions are similar with other molecules). The Landé g-factor for the ground state is $g_{F=1} = -0.51$, and a magnetic field of $B = 5$ G ($\theta = \pi/2$) leads to a Zeeman splitting of $\Delta_z = |\mu_B g_F B|/\hbar \sim 1.25\Gamma$ for $\Delta m_F = 1$ (Here $\mu_B/\hbar \approx 1.4$ MHz/G).

To check the effect of the magnetic field on the SWAP cooling scheme, we first consider a low laser intensity case, i.e., a small Rabi frequency $\Omega_p = \Omega = 10\Gamma$ for each beam. To fulfill the adiabatic condition $|M_{pq}A_{ij}^{(q)}\Omega_p|^2 \gg \alpha$, we choose the frequency ramp speed $\alpha = 4\Gamma^2$ and the sweeping period $T = 5\Gamma^{-1}$. The ramp frequency should cover the resonant positions for all possible transitions[33], which gives the requirement for the sweeping range αT,

$$\alpha T > 2kv + 2\Delta_z. \tag{8}$$

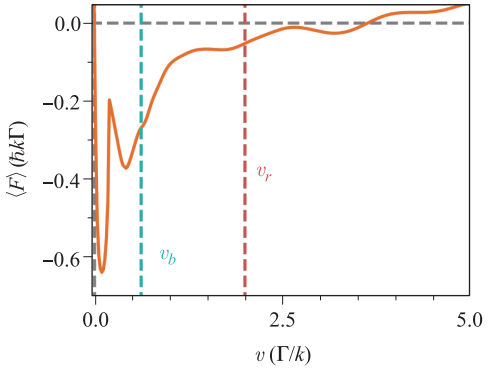

Fig. 2 The cooling force for different velocities of the type-II $F = 1 \to F' = 0$ transition under the SWAP scheme (orange solid line). Here are the parameters we use: $\Omega = 10\Gamma$, $\alpha = 4\Gamma^2$, $T = 5\Gamma^{-1}$ and $B = 5$ G ($\theta = \pi/2$). The critical value of v_b indicated by the cyan dashed line is obtained from Eq. (9), and the red dashed line indicates v_r determined by Eq. (10).

The condition is well fulfilled for velocities shown in Fig. 2.

The cooling force has been enhanced in the small velocity range, as shown in Fig. 2. We label the critical velocity that characters this regime as v_b. To determine v_b, let us analyze the different cooling mechanisms for large and small velocities in the SWAP scheme for the $F = 1 \to F' = 0$ transition. For a relatively small velocity, the Doppler shift $\Delta_D = kv$ is smaller than the Zeeman shift Δ_z, as shown in Fig. 3(a), the time sequence of the stimulated excitation and de-excitation of the three transitions is still in order. At time t_1 in Fig. 3(a), the particles in Zeeman sublevel $m_F = -1$ get excited by the σ^+ component in the counter-propagating beam, then the stimulated de-excitation back to $m_F = -1$ happens at time t_2 with the co-propagating beam. This is similar to the two-level case. As time goes on, this process happens for the other two Zeeman states. However, when t_3 is close to t_2 [see Fig. 3(a)], the de-excitation to the $m_F = 0$ sublevel also happens. Competition between the de-excitation to $m_F = -1$ via the co-propagating beam and to $m_F = 0$ via the counter-propagating beam certainly suppresses the net momentum transfer in one sweeping period. The critical velocity v_b is defined when $t_2 = t_3$. Taking both the Doppler shift and the Zeeman shift into consideration, we have $\omega_0 - \Delta_z + \Delta_D = \omega_0 - \Delta_D$, resulting in

$$v_b = \Delta_z/(2k). \tag{9}$$

In Fig. 2, a rapid decrease of the SWAP cooling force for velocities larger than v_b is consistent with the above discussion.

Moreover, there is an enhanced cooling effect in the small velocity region. The maximum achievable force holds about $\sim 0.6\hbar k\Gamma$, which surpasses the limit that the above mechanism allowed. Such a strong force located near zero velocity should partly attribute to the nontrivial Bragg oscillations, which can induce more than $2\hbar k$ of momentum transfer during one sweeping period. As discussed in Ref. [33], the Bragg effect induced momentum change does not contribute to the cooling process, one should trace this effect out under the dressed state picture. However, these oscillations only play an important role at small velocity regime ($v < 0.1\Gamma/k$) and cause the force displaying an oscillatory behaviour that may restrict the cooling limit. For more details of the cooling behavior in the near-zero velocity regime, we discuss that in Appendix A.1.

When $v_b < v < v_c$, we can depict the physical picture by going to another limit $\Delta_D \gg \Delta_z$, as shown in Fig. 3(b). At time t_1, the σ^+ component in the counter-propagating beam becomes on resonance for the $m_F = -1 \to m'_F = 0$ transition. Since the Doppler shift is large, before the co-propagating beam reaches the resonant point, the de-excitations back to the other two ground sublevels already happen. The π and σ^- components in the counter-propagating beam first become near resonance and drive the stimulated emission processes from $m'_F = 0$ to $m_F = 0$ and $m_F = +1$ respectively. Therefore, the exchanged momenta from excitation and de-excitation are in opposite directions, making the net momentum transfer smaller than $\hbar k$.

Another issue we should pay attention to is the role of the spontaneous emission in the sweeping process. The time order of momentum transfer will be messed up if the stimulated emission is replaced by the spontaneous emission, which would reduce the cooling force. Therefore, an effective SWAP cooling requires a low probability of spontaneous dacay, which means the time interval that a particle spends in the excited state should be less than the lifetime Γ^{-1}. This effect also set an effective cooling velocity range $v < v_r$. For the case in Fig. 3(a) where $\Delta_z \gg \Delta_D$, the time interval $\tau_e = t_2 - t_1 = 2\Delta_D/\alpha$. On the other hand, when $\Delta_D \gg \Delta_z$, they are $\tau_{e1} = t_3 - t_1 = \Delta_z/\alpha$ and $\tau_{e2} = t_2 - t_4 = 2(\Delta_D - \Delta_z)/\alpha$. To guarantee all of the time intervals to fulfill the condition that $\tau_e < 1/\Gamma$, the velocity must be smaller than the upper limit v_r, where

$$v_r = \alpha/(2k\Gamma). \tag{10}$$

Although we only discuss the SWAP cooling on the

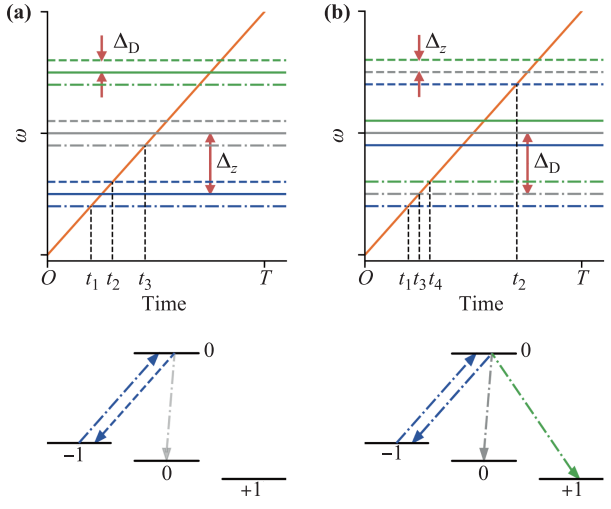

Fig. 3 Resonant time for each polarization component in the two beams for the case of: **(a)** $\Delta_z \gg \Delta_D$ and **(b)** $\Delta_D \gg \Delta_z$. The solid lines represent the resonant frequencies of the three transitions without considering the Doppler effect. The three polarizations are depicted in different colors: σ^+ in blue, π in gray, and σ^- in green. The dashed lines (dotted dashed lines) indicate the resonant time of the three polarization components in the co-propagating (counter-propagating) beam, all shift $+\Delta_D$ $(-\Delta_D)$ compared to the solid lines. t_1 (t_2) is the time when the σ^+ component in the counter-propagating (co-propagating) beam becomes resonant with the $m_F = -1 \to m'_F = 0$ transition. t_3 (t_4) is the time when the π (σ^-) component in the counter-propagating beam becomes resonant with the $m_F = 0(+1) \to m'_F = 0$ transition. The excitation and de-excitation processes after $t_1$are schematically plotted below respectively. The linestyles have the same meanings with those in upper panels.

$F = 1 \rightarrow F' = 0$ transition, the results for other type-II transitions are similar. The complex multi-level system can always be decomposed into several two-level subsystems if the magnetic field is large enough. And the particle will experience similar dynamics with absorption and stimulated emission in one sub-system. So we conclude that, in a multi-level transition, an excitation by the counter-propagating beam must be followed by an emission stimulated by the co-propagating beam to ensure a large momentum transfer. Anything that breaks the order will degrade the cooling effect. In order to achieve a better performance of the SWAP cooling, a relatively strong magnetic field is preferred to meet the condition that $\Delta_z \gg \Delta_{\mathrm{D}}$. This also gives an ideal velocity range that $|v| \ll v_b \leq v_r$, where the cooling effect is significantly enhanced. Of course, larger Zeeman shifts require larger sweeping range as to higher power of cooling lasers to ensure the adiabatic condition.

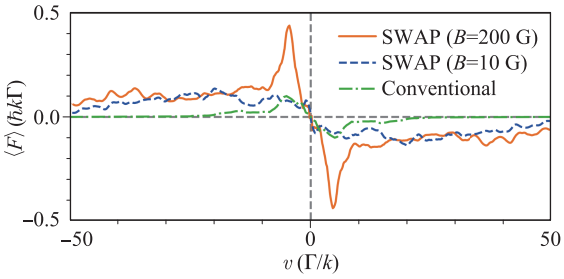

Fig. 4 Comparisons of the SWAP forces to the conventional Doppler cooling force for the ^{138}BaF molecule. Under a weak magnetic field of $B = 10$ G ($\theta = \pi/2$) (blue dashed line), the SWAP parameters are: $\Omega = 100\Gamma$, $\alpha = 100\Gamma^2$, $T = 3\Gamma^{-1}$, $\Delta = +7\Gamma$. With a strong magnetic field of $B = 200$ G (orange solid line), the SWAP parameters are: $\Omega = 50\Gamma$, $\alpha = 160\Gamma^2$, $T = 4\Gamma^{-1}$, $\Delta = -25\ \Gamma$. The parameters used for conventional Doppler cooling (green dotted dashed line) are: $\Omega = 5\Gamma$, $\Delta = -5\Gamma$, $B = 5$ G ($\theta = \pi/2$), and a 38 MHz sideband modulation is applied to cover all hyperfine states for the ^{138}BaF molecule.

4 SWAP cooling for molecules

The results in the type-II transition in Section 3 indicate that application of the SWAP scheme on molecules might be possible. Just as an example, and for checking the conclusions derived above, we perform a numerical calculation for a real molecule (BaF). Without the external magnetic field, the energy gap Δ_{hf} between the $F = 1^{(-)}$ state and the $F = 2$ state is about $\sim 56\Gamma$ for the ^{138}BaF molecule [20]. To avoid the population accumulating into sublevels that are dark, we have to sweep over all lower manifolds. It is almost impossible to apply a scheme that sweep over part of the manifolds and repump from the other, as the hyperfine splitting of the $X^2\Sigma_{1/2}, N = 1$ for ^{138}BaF is not that large enough to guarantee that the molecule get cooling through SWAP without interacting with the repump laser. Therefore, a large frequency sweeping range αT and a large total Rabi frequency Ω are required. Again, we first consider the case with a weak magnetic field $B = 10$ G. The Zeeman shift $\Delta_z = \mu_B B m_F g_F$ is much smaller than the hyperfine splitting Δ_{hf}. As shown in Fig. 4, even with $\Omega = 100\Gamma$, the maximum SWAP force is about $0.1\hbar k\Gamma$, at the same magnitude with that for the conventional Doppler cooling. Although the enhancement does not appear, a wider coolable velocity region is still observed. It can be estimated from Eq. (10) that $v_r \sim 50\Gamma/k$ with $\alpha = 100\Gamma^2$, which indicates the effective cooling range.

The behaviours of the SWAP force under a large magnetic field are different; see Fig. 4. Compared with low field condition, the maximum achievable cooling force is $4\times$ larger, that is, $\sim 0.4\hbar k\Gamma$. The enhanced cooling velocity limit v_b is determined by the energy gaps between every two neighbouring sublevels, as discussed in Section 3. Note that in real molecules, the behaviours of the transition strength and the Zeeman splitting under a large magnetic field different from that under a weak magnetic field. One must take a different quantum label system and recalculate the Zeeman splitting; please see the Appendix A.2 for more details. The energy gaps between the neighbouring Zeeman sublevels maintain around $\sim 15\Gamma$ at $B = 200$ G, leading to $v_b \sim 7.5\Gamma/k$, which is consistent with the result in Fig. 4. On the other hand, the SWAP force has a weak velocity sensitivity, and the cooling forces for large velocities are similar to those with $B = 10$ G, approximate $\sim 0.1\hbar k\Gamma$.

5 Resistance to leakage channels

For molecules, the closed cycling transitions generally can not be perfectly realized due to the existence of the leakage channels, such as the higher vibrational states and the intermediate Δ state [20, 38]. Since the SWAP cooling scheme employs the stimulated emission to transfer the excited particles back to the ground state, the fraction of spontaneous decay gets partially suppressed. Hence, compared to the conventional Doppler cooling, a smaller loss to the possible leakage channels might be expected. In order to understand such an effect, we analyse a simple three-level system, i.e., a two-level transition driven by the frequency-chirped cooling lasers with an additional loss channel (the leakage branch ratio is assumed to be $\gamma = 0.05$) with our semi-classical model in Section 2; see Fig. 5(a). In the conventional Doppler cooling, $\gamma = 0.05$ allows a maximum scattering photon number of $\gamma^{-1} \sim 20$ before the particles populate the leakage state. As shown in Fig. 5(b), with an evolution time of $50\Gamma/k$, the loss fraction reaches ~ 0.7 after scattering ~ 14 photons. However, under the SWAP scheme, with an equivalent evolution time, i.e., five sweeping periods, the loss ℓ_{SWAP} is

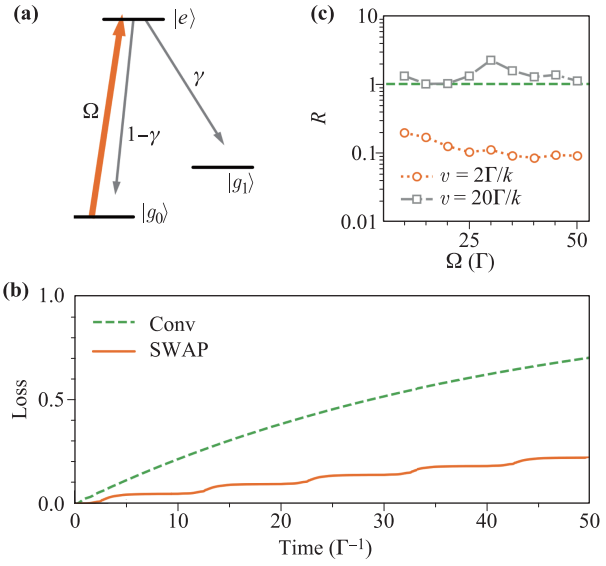

Fig. 5 The resistance of the SWAP cooling scheme on the leakage channels. **(a)** A schematic plot of a two-level system $|g_0\rangle \rightarrow |e\rangle$ driven by a pair of cooling laser beams (Rabi frequency Ω) with an additional dark state $|g_1\rangle$. The leakage branch ratio is γ. **(b)** The population loss to $|g_1\rangle$ within an evolution time of $50\Gamma^{-1}$. Initially, all particles are assumed to populate in the $|g_0\rangle$ state, and $\gamma = 0.05$. For conventional Doppler cooling (green dashed line), $\Omega = 5\Gamma$, the detuning $\Delta = -kv$ with v the velocity of the moving particle. The loss phenomena under the SWAP scheme ($\Omega = 20\Gamma$, $\alpha = 40\Gamma^2$, $T = 10\Gamma^{-1}$) with a velocity of $2\Gamma/k$ is different and shown in orange solid line. **(c)** The dependence of the loss ratio R of the SWAP cooling on Ω for the small ($v = 2\Gamma/k$, orange circles) and large ($v = 20\Gamma/k$, gray squares) velocities.

several times smaller.

To quantitatively evaluate the resistance of the SWAP cooling to the leakage, we introduce a loss ratio defined by

$$R = r_{\mathrm{SWAP}}/r_{\mathrm{Conv}}. \tag{11}$$

Here r_{SWAP} indicates the population loss in the SWAP cooling once the moving particle changing its momentum by $-\hbar k$, resulting a definition as $r_{\mathrm{SWAP}} = \ell_{\mathrm{SWAP}}\hbar k/\delta p_{\mathrm{SWAP}}$ with $\delta p_{\mathrm{SWAP}}(\tau) = |\int_0^\tau \langle F(t)\rangle \mathrm{d}t|$. In the conventional Doppler cooling, $r_{\mathrm{Conv}} \sim \gamma$. Figure 5(c) shows the loss ratios R for two different velocities with various Ω under the SWAP scheme. For a large velocity, for example, $v = 20\Gamma/k$, the ratios are always larger than one, which means that the cooling effect of the SWAP scheme is less significant than the conventional Doppler case as less momenta (~ 10 photons for five periods) are transferred but the loss lies in a similar or larger level. This can be easily understood by introducing the interval time $\tau_e \equiv 2kv/\alpha$ that the particle spends in the excited state. For the parameters we use here, it is estimated to be $\tau_e \sim 1/\Gamma$. Considering the lifetime of the particle $\tau_n = 1/\Gamma$, the effect of swap scheme would be similar to that of the Doppler cooling, which explains the loss ratio $R \sim 1$.

For a small velocity, $v = 2\Gamma/k$, the loss ratio is typically around ~ 0.1. The SWAP scheme is much better compared with the conventional scheme. The reason lies in that, for a small velocity, τ_e is small enough to suppress the spontaneous decay and make the stimulated emission dominate. For $v = 2\Gamma/k$, τ_e happens to be $1/(10\Gamma)$. Considering the ideal case that no spontaneous decay happens and $\delta p_{\mathrm{SWAP}} \sim 2\hbar k$, r_{SWAP} is about $\gamma/20$, leading to the loss ratio $R \sim 0.05$. However, the effect is weakened due to the non-zero Γ. We can also find that with a better fulfillment of the adiabatic condition $\Omega^2 \gg \alpha$ by increasing Ω, the ratio R decreases but always larger than the limit $R = 0.05$, as shown Fig. 5(c). To get a suppression of the spontaneous decay and consequently achieve an effective SWAP cooling, the condition $v \ll \alpha\Gamma^{-1}/(2k)$ should be fulfilled. We claim here that, compared to the conventional Doppler cooling, a better resistance to the leakage channels in the SWAP cooling occurs in the small velocity region, i.e., $v \ll \alpha\Gamma^{-1}/(2k)$.

In the real molecular cooling experiment, scattering of thousands of photons is required, indicating that the vibrational repumping is still needed in the SWAP scheme. For the system in Fig. 5, a loss ratio of $R \sim 0.1$ generally means that only about a hundred of photons are scattered before the particle all populates the $|g_1\rangle$ state. This tells us that the SWAP scheme still leads to non-negligible losses to the $v = 1$ vibrational state, i.e., one should work with at least one extra $v = 1$ vibrational repumping laser, but might get rid of the $v = 3$ and even $v = 2$ repumpers.

6 Conclusion

In summary, we have analyzed the SWAP cooling force for the multi-level type-II transitions and further diatomic molecules. The magnetic field that has an angle θ to the axis of laser beams cannot only remix the Zeeman dark states in the type-II transitions, but also introduce an enhancement to the SWAP cooling force at the small velocity region. When the Zeeman energy splitting is larger than the Doppler shift, the multi-level system can be decomposed into several two-level sub-systems in time ordering. Ideally, a momentum transfer of twice the photon momentum during one sweeping period is allowed and results in an enhanced cooling force for velocities below v_b.

The SWAP scheme does not require a sideband modulation, and is less sensitive to the long-term stabilization of the laser frequency. Unlike the bichromatic cooling, the frequencies of co- and counter-propagating beams of the SWAP scheme have no difference in the laboratory frame and can be done with a retro-reflected mirror. Such properties indicate an easier experimental realization, and the applications in laser slowing of a molecular beam might be possible as well if one can get access to both a high laser

intensity and a rapid frequency ramp speed. For SWAP, the cooling force relies on stimulated emissions and the spontaneous emission rate is reduced, causing the resistance of the leakage channels. This will be useful to reduce the number of the vibrational repump lasers needed for an ordinary molecule that lacks a closed-cycling transition. Also, due to the independence on the spontaneous emission of the SWAP cooling, it will be beneficial for the narrow linewidth transition, which lacks large number of scattered photons, to provide an effective cooling force [29, 33].

Acknowledgements We acknowledge the support from the Natural Science Foundation of Zhejiang Province under Grant No. LZ18A040001, the National Key R&D Program of China under Grant No. 2018YFA0307200, the National Natural Science Foundation of China under Grant No. 12074337, Zhejiang Province Plan for Science and Technology No. 2020C01019, and the Fundamental Research Funds for the Central Universities.

A.1 SWAP cooling in small velocity regime

A.1.1 Dressed-state treatment

For particles with a small momentum, the Bragg oscillation plays an important role in the SWAP process but makes no contribution to the cooling effect, as discussed in Ref. [33]. To exclude this Bragg effect, we work with a Hamiltonian under the dressed state picture as

$$\begin{aligned} H_{\mathrm{D}} =& \sum_p \sum_u \left(\frac{p^2}{2m} + \hbar\Delta^{u,u_0} \right) |u,p\rangle\langle u,p| \\ &+ \sum_p \sum_l \left[\frac{p^2}{2m} + \hbar(\Delta^{u_0,l_0}(t) + \Delta^{l,l_0}) \right] |l,p\rangle\langle l,p| \\ &+ \sum_p \sum_{u,l} \sum_{n,q} \frac{\hbar}{2} \tilde{\Omega}_{ul}^{nq} (|u,p+\hbar k_n\rangle\langle l,p| + h.c.), \end{aligned} \tag{A.1}$$

where we have used the transformation $\mathrm{e}^{\pm \mathrm{i}kz} = \int \mathrm{d}p |p \pm \hbar k\rangle\langle p|$. Here, $\tilde{\Omega}_{ul}^{nq} = M_{nq} A_{ul}^{(q)} \Omega_n$ is time independent, and $k_n = \pm k$ for one-dimensional case. We label the energy gap between $|u\rangle$ and $|u_0\rangle$ and that between $|l\rangle$ and $|l_0\rangle$ as Δ^{u,u_0} and Δ^{l,l_0} respectively. The laser frequencies $\omega_n(t) = \omega(t)$ of the two beams are centered at a frequency ω_{l_0,u_0} on resonance with the transition $|l_0\rangle \leftrightarrow |u_0\rangle$ (note that $|l_0\rangle$ and $|u_0\rangle$ should not necessarily be real energy levels, they can also be virtual and just define a frequency value as a reference for other Zeeman sublevels), and we define $\Delta^{u_0,l_0}(t) = \omega(t) - \omega_{l_0,u_0}$.

Then let us turn to the spontaneous emission. For one-dimensional case, we focus on the momentum change along the $\hat{z}$ direction. The spontaneous decay is contributed by emitting photons with momentum $\hbar k'$ along the $\hat{z}$ axis and angular momentum $\hbar q$. Here k' varies from $-k$ to k, and $q = 0, \pm 1$ corresponds to the $\pi, \sigma^{\pm}$ polarization, and the emitting probability is $N_q(k')$ [39]. The Linblad operator to describe such a progress is

$$\begin{aligned} \hat{\mathcal{L}}_{\mathrm{D}}(\hat{\rho}) =& -\frac{1}{2}\Gamma \sum_p \sum_u (|u,p\rangle\langle u,p|\hat{\rho} + \hat{\rho}|u,p\rangle\langle u,p|) \\ &+ \Gamma \sum_p \sum_{u,l} \sum_q \int_{-k}^{k} \mathrm{d}k' |A_{ul}^{(q)}|^2 N_q(k') |l,p-\hbar k'\rangle \\ &\times \langle u,p|\hat{\rho}|u,p\rangle\langle l,p-\hbar k'|. \end{aligned} \tag{A.2}$$

To simplify the calculation, we choose a coarse discretization of the momentum distribution with a step size $\hbar k$, resulting in $k' = -k, 0, k$. Following Ref. [39], we simply use $N_q(-k) : N_q(0) : N_q(k) = \frac{1}{5} : \frac{3}{5} : \frac{1}{5}$ for all possible q. Then we have

$$\begin{aligned} \hat{\mathcal{L}}_{\mathrm{D}}(\hat{\rho}) =& \frac{1}{2} \sum_p \sum_{u,l} \sum_{k'} (2\hat{C}_{u,l}^{(k')} \hat{\rho} \hat{C}_{u,l}^{(k')\dagger} - \hat{C}_{u,l}^{(k')\dagger} \hat{C}_{u,l}^{(k')} \hat{\rho} \\ &- \hat{\rho} \hat{C}_{u,l}^{(k')\dagger} \hat{C}_{u,l}^{(k')}) \end{aligned} \tag{A.3}$$

with the collapse operator

$$\hat{C}_{u,l}^{(k')} = \sum_q \sqrt{\Gamma N_q(k')} A_{u,l}^{(q)} |l,p-\hbar k'\rangle\langle u,p|. \tag{A.4}$$

Now the time evolution of the system in both the internal states and the momentum space can be described by performing a Monte Carlo simulation [39] with the time-dependent Hamiltonian H_{D} and the $\hat{C}_{u,l}^{(k')}$ operators above.

A.1.2 Simulation results

Here we focus on the SWAP cooling on particles with small momenta, on the magnitude of tens of $\sim \hbar k$, where the motion of particles should be treated under the dressed-state picture as aforementioned. The Monte Carlo simulation is performed with an initial state $|\psi_i\rangle = \sum_l \alpha_l |l,p_0\rangle$, where α_l gives the initial amplitude in the ground state $|l\rangle$ (For simplicity, we assume a uniform distribution that, for example, $\alpha_l = 1/\sqrt{3}$ for the $F = 1 \to F' = 0$ transition.), and p_0 is the initial momentum. Then we evolve this state in the Hilbert space $|i\rangle \otimes |p\rangle$ ($|i\rangle$ indicates the internal state space) for several sweeping periods till the internal state becomes quasi-steady [33], i.e., the populations in each internal sublevel before one sweep equals with those at the end of one sweep. To exclude the effect of Bragg oscillation, we use the root-mean-square momentum $p_{\mathrm{rms}} = \sqrt{\langle\psi|\hat{p}^2|\psi\rangle}$ to describe the cooling process, which in reality reflects the kinetic energy of the particles.

Again we concentrate on the SWAP cooling effect for particles with small momenta in type-II $F = 1 \to F' = 0$ transition. With the semi-classical treatment, a large force in the small velocity region has been shown in Fig. 2, which is, however, partly contributed by the Bragg oscillation. Since the kinetic energy of the particles does not change

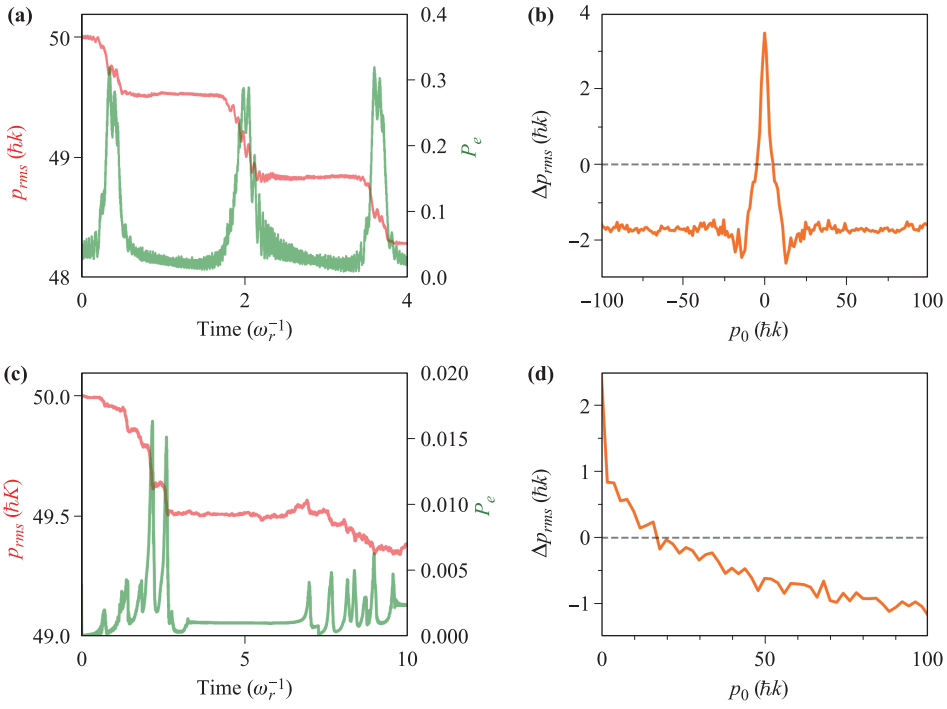

Fig. A1 SWAP cooling on the type-II transition and ^{138}BaF molecule in small velocity regime. **(a)** Time evolution of p_{rms} (red line) and the population in the excited state, P_e (green line), for the $F = 1 \to F' = 0$ transition. The initial momentum of the particle is $p_0 = 50\hbar k$. **(b)** The change of the root-mean-square momentum Δp_{rms} in one sweeping period for varying initial momentum p_0 in the $F = 1 \to F' = 0$ transition. **(c)** Time evolution of p_{rms} (red line) and P_e (green line) at an initial momentum $p_0 = 50\hbar k$ for ^{138}BaF molecules. **(d)** Δp_{rms} in one sweeping period for ^{138}BaF molecules.

after such an oscillation happens, i.e., transfer between $\pm n\hbar k$ (n is an integer), we monitor the change of the root-mean-square momentum $p_{\rm rms}$ and the population in the excited state, $P_e = \sum_{u,p}\langle u,p|u,p\rangle$, during the sweeping. The Rabi frequency $\Omega = 200\omega_r$, the ramp speed $\alpha = 1000\ \omega_r^2$ and the sweeping period $T = 4\omega_r^{-1}$ [$\hbar\omega_r = \frac{(\hbar k)^2}{2m}$ is the photon recoil energy]. Similarly, we still apply an angled magnetic field $B = 25$ G ($\theta = \pi/2$) to destabilize the dark state and also make the stimulated excitation-deexcitation in order ($\Delta_z \gg \Delta_{\rm D}$). The decay rate of the excited state is set to be $\Gamma = \omega_r$.

Figures A1(a) and (b) show the results of SWAP cooling on the $F = 1 \to F' = 0$ transition. We can observe three peaks of the population for the excited state P_e in Fig. A1(a), corresponding to the three excitation-deexcitation processes (see Fig. 3 in the main text). At the same time, the $p_{\rm rms}$ decreases for three times. Our explanation in Fig. 3 is clearly demonstrated here. The reason why the change of p_{rms} less than $2\hbar k$ is attributed to the spontaneous emission for the non-vanishing Γ. Figure A1(b) shows that, the change for root-mean-square momentum, $\Delta p_{rms} = \sqrt{\langle\hat{p}^2\rangle_f} - \sqrt{\langle\hat{p}^2\rangle_i}$, in one sweeping period for various initial momentum p_0. For $|p_0| > 12\hbar k$, Δp_{rms} is approximately $-2\hbar k$, indicating an effective cooling as the kinetic energy decreases. For $|p_0| < 6\hbar k$, heating effect appears. The time order of the excitation-deexcitation processes breaks down for particles whose momentum is close to zero, and there may exist multi-photon procedure that together leads to the heating. This predicts that the SWAP cooling has a temperature limit, which is determined by the Rabi frequency Ω of the beams [28, 33].

Similarly, Figs. A1(c) and (d) show the dynamics of how our SWAP scheme works on molecules in the near-zero velocity region. We still apply a large magnetic field ($B = 100$ G, $\theta = \pi/2$) to separate the hyperfine levels of the molecule apart. The sweeping range is large enough to cover all of the ground-state sublevels by setting $\alpha = 4600\omega_r^2$ and $T = 10\omega^{-1}$. Other parameters are $\Omega = 400\omega_r$ and $\Gamma = 265.4\omega_r$. Figure A1(c) presents that the root-mean-squared momentum experiences decreases two times as the laser frequency sweeps through the two $m_S = \pm 1/2$ manifolds (see Fig. A2). Due to the complicated structure of BaF molecule and the short living lifetime of the excited states, the decrease of p_{rms} in one sweeping period is only about $0.61\hbar k$. It indicates that the scheme may perform better on molecules with a narrow linewidth, for example, the Δ state in YO [40] and BaF [20]. Figure A1(d) shows this cooling effect for different initial momenta up to $100\hbar k$. For the ^{138}BaF molecule, a momentum of $100\hbar k$ is corresponding to a velocity ~ 0.3 m/s, much smaller than $\Gamma/k \sim 2.4$ m/s. The heating effect appears for $|p_0| < 20\hbar k$ with the parameters used here, while for larger p_0, SWAP cooling plays a role

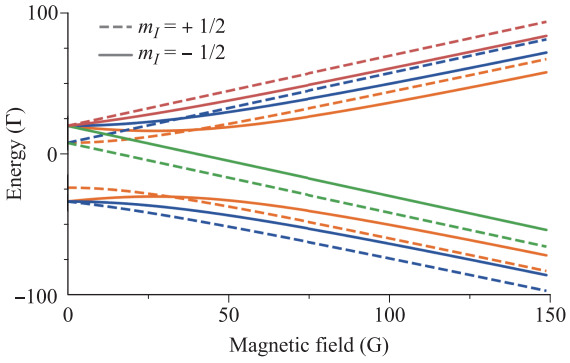

Fig. A2 Energy splittings of the $X^2\Sigma_{1/2}, N = 1$ (N is the roational number) states of the ^{138}BaF molecule under the external magnetic field. The hyperfine states are labeled with $|S, m_S; N, m_N; I, m_I\rangle$. $m_I = +1/3$ and $m_I = -1/2$ are plotted with dashed and solid lines respectively, while different values of m_S and m_N are shown in four different colors: $m_S = -1/2, m_N = -1$ (green), $m_S = -1/2, m_N = 0$ (orange, lower), $m_S = -1/2, m_N = +1$ (blue, lower) and $m_S = +1/2, m_N = +1$ (red), $m_S = +1/2, m_N = 0$ (blue, upper), $m_S = +1/2, m_N = -1$ (orange, upper). The lower four states belong to $J = 1/2$ branch while others are in $J = 3/2$ branch.

and finally leads to a stable decrease of p_{rms}. The Bragg oscillation, however, only dominates in very small momentum region $\sim 20\hbar k$, which is far from the velocity range we concerned in Section 3 and Section 4. The results show an equilibrium temperature of $T_s = \frac{(16\hbar k)^2}{2mk_B}$ [k_B is the Boltzmann constant], which approximates the Doppler limit $T_D = \hbar\Gamma/(2k_B)$. However, if we bring down the Rabi frequency Ω, the temperature T_s would decrease correspondingly until the adiabatic condition $\alpha \ll \Omega^2$ breaks down. The cooling limit of SWAP is predicted to be the recoil temperature $T_r = \hbar\omega_r/k_B$ [33]. Though there are approaches to go beyond this recoil limit such as optical pumping into a velocity-selective dark state [41] or Raman cooling [42], the advantage of the SWAP scheme lies on the strong and stable cooling force on a wide velocity range for atoms and molecules rather than a possible lowest temperature.

A.2 Transition strength and Zeeman splitting of molecules under larger magnetic field

A.2.1 Zeeman splitting of ^{138}BaF molecule

Figure A2 shows the Zeeman splitting of the ground state $|X^2\Sigma_{1/2}, N = 1\rangle$ of ^{138}BaF molecule under different strength of the magnetic field. More details about the structure of the ^{138}BaF molecule can be found in Ref. [20]. The energy shift for each sublevel approximately varies in parallel with each other in the same m_S branch as the magnetic field strength becomes larger. To ensure a large enough energy gap which is essential for our scheme in Section 4, the magnetic field should be no less than 100 G. For molecules under a small magnetic field, e.g., $B < 20$ G, the total angular momentum F remains the good quantum number, while for the case of a large magnetic field we apply here, the electron spin S decouples from the nuclear angular momenta I and rotational angular momenta N. Therefore, we label the eigenstates with $|S, m_S; I, m_I; N, m_N\rangle$ instead of $|J, F, m_F\rangle$ since F is no longer a good quantum number.

A.2.2 Derivation of the matrix elements of the electric dipole transitions under large magnetic field

Following the labels used in Ref. [20] and Ref. [43], the ground state in fully decoupled form can be written as

$$\begin{aligned}|g\rangle &= |\Lambda; S, m_S; N, m_N; I, m_I\rangle \\ &= \sum_{J,m_J}\sum_{\Sigma}(-1)^{S-N+m_J+J+\Omega}\sqrt{(2J+1)(2N+1)} \\ &\quad\times \begin{pmatrix} N & S & J \\ m_N & m_S & -m_J \end{pmatrix}\begin{pmatrix} N & S & J \\ \Lambda & \Sigma & -\Omega \end{pmatrix} \\ &\quad\cdot |\Lambda; S, \Sigma; J, \Omega, m_J\rangle|I, m_I\rangle, \end{aligned} \tag{A.5}$$

while the excited state in Hund's case is

$$\begin{aligned}|e\rangle &= ||\Lambda'|; J', m'_J; I', m'_I; +\rangle \\ &= \frac{1}{\sqrt{2}}(|\Lambda'; S', \Sigma'; J', \Omega', m'_J\rangle + (-1)^{J'-S'} \\ &\quad\cdot |-\Lambda'; S', -\Sigma'; J', -\Omega', m'_J\rangle)|I', m'_I\rangle. \end{aligned} \tag{A.6}$$

Then, the matrix element for electric dipole transition from $|g\rangle$ to $|e\rangle$ is

$$\begin{aligned}\langle d\rangle &= \langle e|T^1_p(\hat{d})|g\rangle \\ &= \frac{1}{\sqrt{2}}\delta_{I,I'}\delta_{m_I,m'_I}\sum_{J,m_J}\sum_{\Sigma}(-1)^{S-N+m_J+J+\Omega} \\ &\quad\times\sqrt{(2J+1)(2N+1)}\begin{pmatrix} N & S & J \\ m_N & m_S & -m_J \end{pmatrix}_s\begin{pmatrix} N & S & J \\ \Lambda & \Sigma & -\Omega \end{pmatrix} \\ &\quad\times(\langle\Lambda'; S', \Sigma'; J', \Omega', m'_J|T^1_p(\hat{d})|\Lambda; S, \Sigma; J, \Omega, m_J\rangle \\ &\quad+\langle-\Lambda'; S', -\Sigma'; J', -\Omega', m'_J|T^1_p(\hat{d})|\Lambda; S, \Sigma; J, \Omega, m_J\rangle). \end{aligned} \tag{A.7}$$

Here $\hat{d}$ is the electric dipole operator, and $T^1_p(\hat{d})$ is a tensor operator for $\hat{d}$.

By applying Wigner–Eckart theorem, the internal term becomes

$$\begin{aligned}&\langle\Lambda'; S', \Sigma'; J', \Omega', m'_J|T^1_p(\hat{d})|\Lambda; S, \Sigma; J, \Omega, m_J\rangle \\ &= \delta_{\Sigma,\Sigma'}\sum_q(-1)^{m'_J-\Omega'}\sqrt{(2J'+1)(2J+1)} \\ &\quad\times\begin{pmatrix} J' & 1 & J \\ -m'_J & p & m_J \end{pmatrix}\begin{pmatrix} J' & 1 & J \\ -\Omega' & q & \Omega \end{pmatrix}\langle\Lambda'|T^1_q(\hat{d})|\Lambda\rangle. \end{aligned} \tag{A.8}$$

Table A1 Calculated matrix elements for electric dipole transitions from $|X, N = 1, -\rangle$ state to $|A, J' = 1/2, +\rangle$ state under a large magnetic field (in natural unit). Here the first column refers to the levels in $|X, N = 1, -\rangle$ state while the first row refers to levels in $|A, J' = 1/2, +\rangle$ state respectively.

			$m'_J = -1/2$	$-1/2$	$+1/2$	$+1/2$
m_S	m_N	m_I	$m'_I = +1/2$	$-1/2$	$-1/2$	$+1/2$
$-1/2$	$+1$	$+1/2$	0.6084	0	0	0.1925
	$+1$	$-1/2$	0	0.6084	0.1925	0
	0	$+1/2$	-0.5443	0	0	-0.1925
	0	$-1/2$	0	-0.5443	-0.1925	0
	-1	$+1/2$	0.4082	0	0	0
	-1	$-1/2$	0	0.4082	0	0
$+1/2$	-1	$-1/2$	0	0.1925	0.6084	0
	-1	$+1/2$	0.1925	0	0	0.6084
	0	$-1/2$	0	-0.1925	-0.5443	0
	0	$+1/2$	-0.1925	0	0	-0.5443
	$+1$	$-1/2$	0	0	0.4082	0
	$+1$	$+1/2$	0	0	0	0.4082

Since matrix element $\langle \Lambda' | T^1_q(\hat{d}) | \Lambda \rangle$ is common for all $\Delta\Lambda = \pm 1$ transitions, we obtain from Eq. (A.7) all possible hyperfine transition strength, i.e., values of A in Eq. (3), in $|X, N = 1, -\rangle \to |A, J = 1/2, +\rangle$ transitions under large magnetic field, as listed in Table A1.

References

1. S. Chu, The manipulation of neutral particles, *Rev. Mod. Phys.* 70(3), 685 (1998)
2. W. D. Phillips, Laser cooling and trapping of neutral atoms, *Rev. Mod. Phys.* 70(3), 721 (1998)
3. C. N. Cohen-Tannoudji, Manipulating atoms with photons, *Rev. Mod. Phys.* 70(3), 707 (1998)
4. E. A. Cornell and C. E. Wieman, Bose–Einstein condensation in a dilute gas, the first 70 years and some recent experiments, *Rev. Mod. Phys.* 74(3), 875 (2002)
5. I. Bloch, J. Dalibard, and W. Zwerger, Many-body physics with ultracold gases, *Rev. Mod. Phys.* 80(3), 885 (2008)
6. A. D. Ludlow, M. M. Boyd, J. Ye, E. Peik, and P. O. Schmidt, Optical atomic clocks, *Rev. Mod. Phys.* 87(2), 637 (2015)
7. J. L. Bohn, A. M. Rey, and J. Ye, Cold molecules: Progress in quantum engineering of chemistry and quantum matter, *Science* 357(6355), 1002 (2017)
8. M. S. Safronova, D. Budker, D. DeMille, D F J. Kimball, A. Derevianko, and C. W. Clark, Search for new physics with atoms and molecules, *Rev. Mod. Phys.* 90(2), 025008 (2018)
9. H. Metcalf, Strong optical forces on atoms in multifrequency light, *Rev. Mod. Phys.* 89(4), 041001 (2017)
10. T. Lu, X. Miao, and H. Metcalf, Bloch theorem on the Bloch sphere, *Phys. Rev. A* 71(6), 061405 (2005)
11. X. Miao, E. Wertz, M. G. Cohen, and H. Metcalf, Strong optical forces from adiabatic rapid passage, *Phys. Rev. A* 75(1), 011402 (2007)
12. A. M. Jayich, A. C. Vutha, M. T. Hummon, J. V. Porto, and W. C. Campbell, Continuous all-optical deceleration and single-photon cooling of molecular beams, *Phys. Rev. A* 89(2), 023425 (2014)
13. J. Söding, R. Grimm, Yu. B. Ovchinnikov, Ph. Bouyer, and Ch. Salomon, Short-distance atomic beam deceleration with a stimulated light force, *Phys. Rev. Lett.* 78(8), 1420 (1997)
14. L. Yatsenko and H. Metcalf, Dressed-atom description of the bichromatic force, *Phys. Rev. A* 70(6), 063402 (2004)
15. M. Partlow, X. Miao, J. Bochmann, M. Cashen, and H. Metcalf, Bichromatic slowing and collimation to make an intense helium beam, *Phys. Rev. Lett.* 93(21), 213004 (2004)
16. C. Corder, B. Arnold, and H. Metcalf, Laser cooling without spontaneous emission, *Phys. Rev. Lett.* 114(4), 043002 (2015)
17. E. S. Shuman, J. F. Barry, and D. DeMille, Laser cooling of a diatomic molecule, *Nature* 467(7317), 820 (2010)
18. M. T. Hummon, M. Yeo, B. K. Stuhl, A. L. Collopy, Y. Xia, and J. Ye, 2D magneto-optical trapping of diatomic molecules, *Phys. Rev. Lett.* 110(14), 143001 (2013)
19. M. D. Di Rosa, Laser-cooling molecules, *Europ. Phys. J. D* 31, 395 (2004)
20. T. Chen, W. Bu, and B. Yan, Structure, branching ratios, and a laser-cooling scheme for the ^{138}BaF molecule, *Phys. Rev. A* 94(6), 063415 (2016)
21. B. K. Stuhl, B. C. Sawyer, D. Wang, and J. Ye, Magneto-optical trap for polar molecules, *Phys. Rev. Lett.* 101(24), 243002 (2008)
22. T. Chen, W. Bu, and B. Yan, Radiative deflection of a BaF molecular beam via optical cycling, *Phys. Rev. A* 96(5), 053401 (2017)
23. I. Kozyryev, L. Baum, L. Aldridge, P. Yu, E. E. Eyler, and J. M. Doyle, Coherent bichromatic force deflection of molecules, *Phys. Rev. Lett.* 120(6), 063205 (2018)
24. H. Metcalf and P. V. der Straten, Laser Cooling and Trapping, Springer, 1999
25. J. Dalibard and C. Cohen-Tannoudji, Laser cooling below the Doppler limit by polarization gradients: Simple theoretical models, *J. Opt. Soc. Am. B* 6(11), 2023 (1989)
26. P. Ungar, D. Weiss, E. Riis, and S. Chu, Optical molasses and multilevel atoms: Theory, *J. Opt. Soc. Am. B* 6(11), 2058 (1989)
27. S. A. Malinovskaya and G. Liu, Harmonic spectral modulation of an optical frequency comb to control the ultracold molecules formation, *Chem. Phys. Lett.* 664, 1 (2016)
28. M. A. Norcia, J. R. K. Cline, J. P. Bartolotta, M. J. Holland, and J. K. Thompson, Narrow-line laser cooling by adiabatic transfer, *New J. Phys.* 20(2), 023021 (2018)

29. J. A. Muniz, M. A. Norcia, J. R. K. Cline, and J. K. Thompson, A robust narrow-line magneto-optical trap using adiabatic transfer, arXiv: 1806.00838 (2018)
30. N. Petersen, F. Mühlbauer, L. Bougas, A. Sharma, D. Budker, and P. Windpassinger, Sawtooth-wave adiabatic-passage slowing of dysprosium, *Phys. Rev. A* 99(6), 063414 (2019)
31. J. P. Bartolotta and M. J. Holland, Sawtooth-wave adiabatic passage in a magneto-optical trap, *Phys. Rev. A* 101(5), 053434 (2020)
32. G. P. Greve, B. Wu, and J. K. Thompson, Laser cooling with adiabatic transfer on a Raman transition, *New J. Phys.* 21(7), 073045 (2019)
33. J. P. Bartolotta, M. A. Norcia, J. R. K. Cline, J. K. Thompson, and M. J. Holland, Laser cooling by sawtooth-wave adiabatic passage, *Phys. Rev. A* 98(2), 023404 (2018)
34. A. M. L. Oien, I. T. McKinnie, P. J. Manson, W. J. Sandle, and D. M. Warrington, Cooling mechanisms in the sodium type-II magneto-optical trap, *Phys. Rev. A* 55(6), 4621 (1997)
35. V. B. Tiwari, S. Singh, H. S. Rawat, and S. C. Mehendale, Cooling and trapping of ^{85}Rb atoms in the ground hyperfine $F = 2$ state, *Phys. Rev. A* 78(6), 063421 (2008)
36. L. Anderegg, B. L. Augenbraun, E. Chae, B. Hemmerling, N. R. Hutzler, A. Ravi, A. Collopy, J. Ye, W. Ketterle, and J. M. Doyle, Radio frequency magneto-optical trapping of CaF with high density, *Phys. Rev. Lett.* 119(10), 103201 (2017)
37. S. Truppe, H. J. Williams, M. Hambach, L. Caldwell, N. J. Fitch, E. A. Hinds, B. E. Sauer, and M. R. Tarbutt, Molecules cooled below the Doppler limit, *Nat. Phys.* 13(12), 1173 (2017)
38. M. Yeo, M. T. Hummon, A. L. Collopy, B. Yan, B. Hemmerling, E. Chae, J. M. Doyle, and J. Ye, Rotational state microwave mixing for laser cooling of complex diatomic molecules, *Phys. Rev. Lett.* 114(22), 223003 (2015)
39. K. Mølmer, Y. Castin, and J. Dalibard, Monte Carlo wavefunction method in quantum optics, *J. Opt. Soc. Am. B* 10(3), 524 (1993)
40. A. L. Collopy, M. T. Hummon, M. Yeo, B. Yan, and J. Ye, Prospects for a narrow line MOT in YO, *New J. Phys.* 17(5), 055008 (2015)
41. A. Aspect, E. Arimondo, R. Kaiser, N. Vansteenkiste, and C. Cohen-Tannoudji, Laser cooling below the one-photon recoil energy by velocity-selective coherent population trapping, *Phys. Rev. Lett.* 61(7), 826 (1988)
42. M. Kasevich and S. Chu, Laser cooling below a photon recoil with three-level atoms, *Phys. Rev. Lett.* 69(12), 1741 (1992)
43. J. Brown and A. Carrington, Rotational Spectroscopy of Diatomic Molecules, Cambridge University Press, 2003